Exploration of resonances by using complex momentum representation*

Ya-Juan Tian(田亚娟) Tai-Hua Heng(衡太骅) Zhong-Ming Niu(牛中明)
Quan Liu(刘泉) Jian-You Guo(郭建友)[1)]
School of Physics and Materials Science, Anhui University, Hefei 230601, China

Abstract: Resonance research is a hot topic in nuclear physics, and many methods have been developed for resonances. In this paper, we explore resonances by solving the Schrödinger equation in complex momentum representation, in which the bound states and resonant states are separated completely from the continuum and exposed clearly in the complex momentum plane. We have checked the convergence of the calculations on the grid numbers of the Gauss-Hermite quadrature and the Gauss-Legendre quadrature, and the dependence on the contour of momentum integration. Satisfactory results are obtained. ^{17}O is chosen as an example, and we have calculated the bound and resonant states to be in excellent agreement with those calculated in the coordinate representation.

Keywords: single-particle levels, resonant states, complex momentum representation

PACS: 21.10.Pc, 25.70.Ef, 21.60.-n **DOI:** 10.1088/1674-1137/41/4/044104

1 Introduction

Resonances are one of the most interesting phenomena, and occur widely in nature [1]. There are many types of resonance, including mechanical, acoustic, electromagnetic, nuclear magnetic, electron spin resonance and quantum wave function resonances. Resonances play an important role in the formation of many physical phenomena, such as haloes [2–4], giant haloes [5, 6], deformed haloes [7], and quantum haloes [8]. Therefore, it is very meaningful to study resonances in different fields.

So far, many methods have been developed for resonances. These include the R-matrix method [9], the real stabilization (RSM) method [10], the S-matrix method [11], the J-matrix method [12], the analytic continuation in the coupling constant (ACCC) approach [13], the K-matrix method [14], the Jost function approach [15, 16], and Green's function method [17, 18]. These methods have gained success in handling unbound problems. Even so, physicists hope to establish a unified theory, which can deal with bound states and resonant states on the same footing. The complex scaling method (CSM) introduced in Ref. [19] has partly satisfied this requirement.

In the CSM, the wave functions adopted for resonant states are square-integrable, so it is not necessary to use the asymptotic boundary conditions. Moreover, the complex scaled equation can be solved by using the bound-state methods, in which the bound states and resonant states are processed equally. These advantages enable the application of the CSM to different theoretical frameworks, including combinations with the few-body model [20], shell model [21, 22], and Hartree-Fock theory [23, 24]. More applications of the CSM can be found in Refs. [25–27]. Recently, we have applied the CSM to the relativistic framework [28], and explored the resonant states in spherical nuclei [29, 30] and deformed nuclei [31]. The results are compared with those obtained by other methods and found to have satisfactory agreement [32, 33].

Although the CSM can provide a unified description for bound states and resonant states, there are still some shortcomings. To determine accurately the resonance parameters, repeated diagonalization of the Hamiltonian is required in the complex scaling calculations. The calculated results are not completely independent of the complex rotation angle, which is an unphysical parameter. In addition, the CSM is applicable to only the dilation analytic potential. For systems like nuclei, the mean-field for nucleon movement is similar to a Woods-Saxon potential. There is a singularity when the complex

Received 29 September 2016

∗ Supported by National Natural Science Foundation of China (11575002, 11175001, 11205004, 11305002), Program for New Century Excellent Talents at the University of China (NCET-05-0558), Natural Science Foundation of Anhui Province (1408085QA21), Key Research Foundation of Education Ministry of Anhui Province of China (KJ2016A026), and 211 Project of Anhui University

1) E-mail: jianyou@ahu.edu.cn

rotation angle $\theta = \tan^{-1}(\pi a/R)$. Hence, the CSM is only effective in the interval of $0 < \theta < \tan^{-1}(\pi a/R)$ for resonances in nuclei, which confines the application of the CSM to very broad resonances.

In order to keep the advantages of the CSM without its shortcomings, a complex momentum representation (CMR) method has been established for resonant states [34–36], in which the Schrödinger equation is represented in momentum space. The bound states can be obtained by solving the Schrödinger equation in real momentum space [37, 38]. When the Schrödinger equation is solved in the complex momentum space, all the bound and resonant states can be obtained simultaneously. This method has avoided all the defects of the CSM, and can describe bound states and resonant states on an equal footing. In addition, this method is a bound-state-type method, and can conveniently be applied to other fields. With these advantages, this method has been applied to the investigation of exotic nuclei [39, 40]. Recently, we have combined the relativistic mean field (RMF) with the complex momentum representation (CMR) and established the RMF-CMR method for resonances in nuclei [41].

Until now, we have not found the details of this method regardless of the relativistic or non-relativistic case. For simplicity and without loss of generality, we choose the Schrödinger equation describing spherical nuclei as an example, with the theoretical formalism presented in detail. We then introduce the numerical details for the bound states and resonant states, and check the convergence of the calculations on several model parameters: the upper truncation of momentum integration $k_{\max}$, the grid number N_l in the Gauss-Legendre quadrature, and the grid number N_h in the Gauss-Hermite quadrature. Taking a particular nucleus as an example, we calculate the energies of bound states and resonant states in comparison with those obtained by the CSM calculations in coordinate representation.

2 Formalism

To introduce the complex momentum representation method for resonances, the Schrödinger equation is written as

$$H|\psi\rangle = E|\psi\rangle, \tag{1}$$

with the Hamiltonian

$$H = T + V, \tag{2}$$

where T is the kinetic energy operator and V is the interaction potential. The kinetic energy operator $T = p^2/2m$ with the mass m and momentum $\vec{p}$ linked to the wavevector $\vec{k} = \vec{p}/\hbar$. Similar to Ref. [42], the adopted interaction potential V consists of the central potential

$$V_{\rm ct}(r) = V_0 f(r), \tag{3}$$

and the spin-orbit coupling

$$V_{\rm sl}(r) = -0.44V_0\left(\vec{l}\cdot\vec{s}\right) r_0^2 \frac{1}{r}\frac{{\rm d}f(r)}{{\rm d}r}, \tag{4}$$

where $f(r)$ is a Woods-Saxon type

$$f(r) = \frac{1}{1+\exp\left(\dfrac{r-R}{a}\right)}. \tag{5}$$

For simplicity, the parameters of the Woods-Saxon potential are taken from the standard ones [42, 43]. Namely, the diffuseness $a = 0.67$ fm and the radius $R = r_0 A^{1/3}$, where $r_0 = 1.27$ fm and A is the mass number of the nucleus. The depth of the Woods-Saxon potential $V_0 = -51 + 33\,(N-Z)/A$ (MeV), with the neutron number N and the proton number Z.

The solutions of Eq. (1) include the spectra of the bound states, the resonant states and the continuum. The bound states can be given by the usual methods. For the resonant states, the momentum representation is adopted with the Schrödinger equation:

$$\int {\rm d}^3\vec{k}'\langle\vec{k}|H|\vec{k}'\rangle\Phi(\vec{k}') = E\Phi(\vec{k}), \tag{6}$$

where $\Phi(\vec{k})$ denotes the momentum wavefunctions, where wavevector $\vec{k}$ refers to momentum. For a spherically symmetric system, the wavefunctions $\Phi(\vec{k})$ are written as

$$\Phi(\vec{k}) = \phi(k)Y_l^m(\Omega_k), \tag{7}$$

where $\phi(k)$ and $Y_l^m(\Omega_k)$ are respectively the radial and angular parts of the momentum wavefunctions. Putting the wavefunctions (7) into equation (6), the Schrödinger equation becomes

$$\frac{k^2}{2m}\phi(k) + \int {\rm d}k'\,k'^2\phi(k')V(k,k') = E\phi(k), \tag{8}$$

with

$$V(k,k') = \frac{2}{\pi}\int {\rm d}r\, r^2 j_l(kr) j_l(k'r), \tag{9}$$

where $j_l(kr)$ is the spherical Bessel function of order l. It is difficult, however, to obtain the solution of the integral equation (8). For this reason, we turn the integration in Eq. (8) into a sum over a finite set of points k_j and ${\rm d}k$ with a set of weights w_j. Because the sum with evenly spaced ${\rm d}k$ and a constant weight w_j converges slowly, we replace the sum by the Gauss-Legendre quadrature with a finite grid number N_l, which gives us a $N_l \times N_l$ matrix equation

$$\sum_{j=1}^{N_l} H_{i,j}\phi(k_j) = E\phi(k_i), \quad (i = 1, 2, \cdots, N_l), \tag{10}$$

where

$$H_{i,j}=\frac{k_i^2}{2m}\delta_{i,j}+w_j k_j^2 V_{i,j}, \tag{11}$$

with

$$V_{i,j}=\frac{2}{\pi}\int \mathrm{d}r\, r^2 V(r) j_l(k_i r) j_l(k_j r). \tag{12}$$

The Hamiltonian matrix in Eq. (11) is not symmetric. For simplicity in computation, we symmetrize the matrix by performing the following transformation

$$\phi'(k_i)=\sqrt{w_i}k_i\phi(k_i), H'_{i,j}=\sqrt{\frac{w_i}{w_j}}\frac{k_i}{k_j}H_{i,j}. \tag{13}$$

Putting Eq. (13) into Eq. (10), we obtain a symmetric Hamiltonian matrix as

$$H'_{i,j}=\frac{k_i^2}{2m}\delta_{i,j}+\sqrt{w_i w_j}k_i k_j V_{i,j}. \tag{14}$$

So far, the solution of the Schrödinger equation (6) has become an eigensolution problem of the symmetric matrix (14). To calculate the symmetric matrix, several key points need to be clarified. At first, it is necessary to determine a proper contour in order to expose all the bound and resonant states concerned. Details can be found in Ref. [41]. When the contour is confined, we need to determine several unphysical parameters to reach satisfactory results. As the integration in Eq. (8) is from zero to infinity, the integration must be truncated to a large enough momentum $k_{\max}$. When $k_{\max}$ is fixed, the integration can be calculated by a sum with an enough grid number N_l in the Gauss-Legendre quadrature. In calculating the potential matrix (12), the coordinate integration is replaced by the Gauss-Hermite quadrature with a high enough grid number N_h for the required precision. In the following, we first discuss the choice of the contour and the determination of parameters, and then explore the bound and resonant states in a particular nucleus.

3 Result and discussion

With the theoretical formalism, we explore the bound and resonant states for a realistic physical system. Taking ^{17}O as an example, we first choose an appropriate contour for the momentum integration, and then determine the three unphysical parameters: the upper truncation of momentum integration $k_{\max}$, the grid number N_l in the Gauss-Legendre quadrature, and the grid number N_h in the Gauss-Hermite quadrature.

To single out a proper contour of the momentum integration, we check the dependence of the calculated results on the contour. In Fig. 1, we show the calculations in four different rectangle contours for the single particle state $1d_{3/2}$. It can be seen that the resonant state $1d_{3/2}$ is separated from the continuum and exposed clearly in the complex momentum plane. In every subfigure, the contour is different. The continuum follows the contour, while the position of the resonant state $1d_{3/2}$ remains unchanged. That is, the resonance is independent of the contour. The position of the resonant state $1d_{3/2}$ in the complex momentum plane is located approximately at the point with $k=0.2897-\mathrm{i}0.0209$ fm^{-1} in every subfigure.

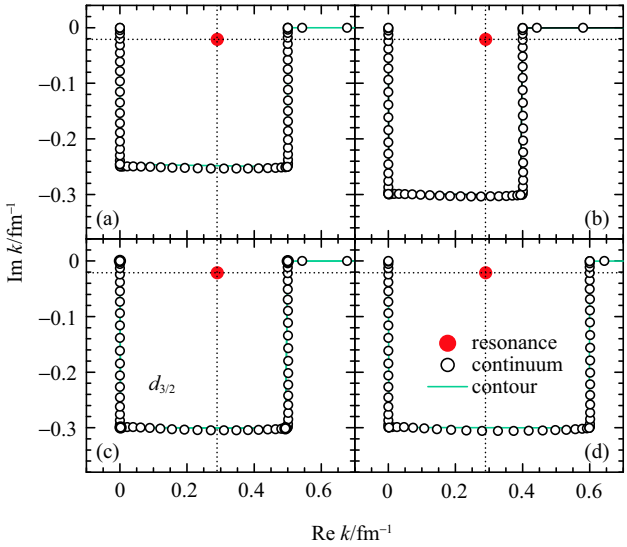

Fig. 1. (color online) The complex momentum solutions of the Schrödinger equation for the state $1d_{3/2}$ in the four different rectangle contours. The red filled circle and the black open circles in every subfigure represent the resonant states and the continuum, respectively.

Besides the rectangle contour, we have also examined the dependence of the calculated results on a triangular contour. The results shown in Fig. 2 are similar to those in Fig. 1. That is, the position of the resonant states is independent of the contour. When the contour is small, only a resonant state $1d_{3/2}$ is exposed in the complex momentum plane (see Fig. 2(a)). With the contour becoming larger, more resonances are exposed in the complex momentum plane. In Fig. 2(b), there are two resonant states, $1d_{3/2}$ and $1f_{7/2}$, exposed in the complex momentum plane. In Fig. 2(c), there are three resonant states, $1d_{3/2}$, $1f_{7/2}$, and $1g_{9/2}$, emerging in the complex momentum plane. This is also observed in Fig. 2(d). For the present system, there are three resonant states. When the contour is added to $k=0$ fm^{-1}, $k=1.0-\mathrm{i}0.4$ fm^{-1}, $k=2.0$ fm^{-1}, and $k_{\max}=5.0$ fm^{-1}, all the resonant states concerned are exposed clearly in the complex momentum plane. Although the contour is different, the position of the resonant states does not move as they are exposed in the complex momentum plane.

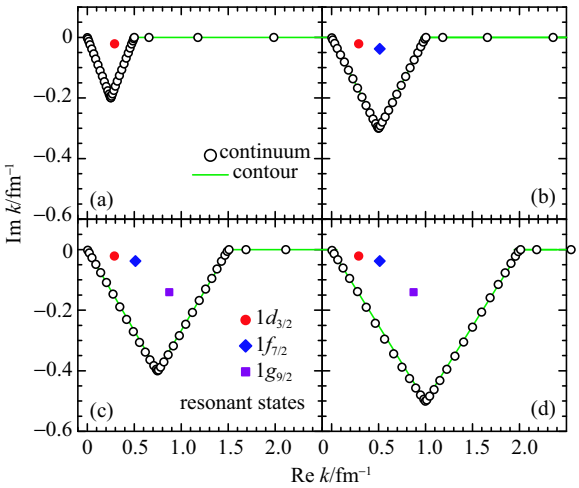

Fig. 2. (color online) The complex momentum solutions of the Schrödinger equation in the four different triangle contours. The red filled circle, blue filled diamond, and violet filled square represent the resonant states $1d_{3/2}$, $1f_{7/2}$, and $1g_{9/2}$, respectively. The black open circles and olive solid line represent respectively the continuum and the contour of integration in the complex momentum place.

As the resonant states are independent of the contour, we can select a large enough contour to expose all the resonances concerned. Using the triangular contour with the four points $k = 0$ fm^{-1}, $k = 1.0 - \mathrm{i}0.5$ fm^{-1}, $k = 2.0$ fm^{-1}, and $k_{\max} = 5.0$ fm^{-1}, we check the dependence of the calculated results on the three unphysical parameters: the upper truncation of momentum integration $k_{\max}$, the grid number N_l in the Gauss-Legendre quadrature, and the grid number N_h in the Gauss-Hermite quadrature, in order to obtain the required precision.

The calculated results with the different upper truncations of the momentum integration $k_{\max}$ are listed in Table 1, with the parameters $N_l = 60$ and $N_h = 70$. From Table 1, the convergence of the calculations on $k_{\max}$ is very good. With the increase of $k_{\max}$ from 2.5 fm^{-1} to 6.0 fm^{-1} by steps of 0.5 fm^{-1}, there is a slight difference in the calculated energy. When $k_{\max} \geqslant 4.0$ fm^{-1}, the calculated results are unchanged in the present precision, which implies that $k_{\max} = 5.0$ fm^{-1} is enough in the present calculations.

Table 1. The single particle energies for the bound and resonant states in ^{17}O varying with the upper truncation $k_{\max}$ of the momentum integration in the present calculations. Here, the grid number $N_l = 60$ for the Gauss-Legendre quadrature of the momentum integration and the grid number $N_h = 70$ for the Gauss-Hermite quadrature in Eq. (12). All energies are in units of MeV and $k_{\max}$ is in units of fm^{-1}

$k_{\max}$	$1s_{1/2}$ E	$2s_{1/2}$ E	$1p_{1/2}$ E	$1p_{3/2}$ E	$1d_{5/2}$ E	$1d_{3/2}$ E_r, E_i	$1f_{7/2}$ E_r, E_i	$1g_{9/2}$ E_r, E_i
2.5	−30.4259	−3.0227	−12.3987	−17.5208	−4.9607	1.8403, −0.2682	5.7737, −0.8611	16.3639, −5.4200
3.0	−30.4270	−3.0244	−12.3998	−17.5242	−4.9634	1.8395, −0.2679	5.7716, −0.8597	16.3678, −5.4016
3.5	−30.4270	−3.0250	−12.4001	−17.5244	−4.9642	1.8393, −0.2678	5.7706, −0.8592	16.3673, −5.4002
4.0	−30.4270	−3.0250	−12.4001	−17.5244	−4.9643	1.8392, −0.2678	5.7706, −0.8592	16.3673, −5.4000
4.5	−30.4270	−3.0250	−12.4001	−17.5244	−4.9643	1.8392, −0.2678	5.7706, −0.8592	16.3673, −5.4000
5.0	−30.4270	−3.0250	−12.4001	−17.5244	−4.9643	1.8392, −0.2678	5.7706, −0.8592	16.3673, −5.4000
5.5	−30.4270	−3.0250	−12.4001	−17.5244	−4.9643	1.8392, −0.2678	5.7706, −0.8592	16.3673, −5.4000
6.0	−30.4270	−3.0250	−12.4001	−17.5244	−4.9643	1.8392, −0.2678	5.7706, −0.8592	16.3673, −5.4000

Table 2. The single particle energies for the bound and resonant states in ^{17}O varying with the grid number N_l of the Gauss-Legendre quadrature of the momentum integration. Here, the upper truncation $k_{\max} = 5.0$ fm^{-1} for the momentum integration and the grid number $N_h = 70$ for the Gauss-Hermite quadrature in Eq. (12). All energies are in unit of MeV.

N_l	$1s_{1/2}$ E	$2s_{1/2}$ E	$1p_{1/2}$ E	$1p_{3/2}$ E	$1d_{5/2}$ E	$1d_{3/2}$ E_r, E_i	$1f_{7/2}$ E_r, E_i	$1g_{9/2}$ E_r, E_i
20	−30.4219	−2.9596	−12.3880	−17.5211	−4.9627	1.8286, −0.3148	5.7469, −0.8353	16.3524, −5.3732
30	−30.4270	−3.0251	−12.4001	−17.5244	−4.9643	1.8363, −0.2648	5.7700, −0.8601	16.3672, −5.4001
40	−30.4270	−3.0250	−12.4001	−17.5244	−4.9643	1.8397, −0.2677	5.7706, −0.8592	16.3673, −5.4000
50	−30.4270	−3.0250	−12.4001	−17.5244	−4.9643	1.8392, −0.2678	5.7706, −0.8592	16.3673, −5.4000
60	−30.4270	−3.0250	−12.4001	−17.5244	−4.9643	1.8392, −0.2678	5.7706, −0.8592	16.3673, −5.4000
70	−30.4270	−3.0250	−12.4001	−17.5244	−4.9643	1.8392, −0.2678	5.7706, −0.8592	16.3673, −5.4000
80	−30.4270	−3.0250	−12.4001	−17.5244	−4.9643	1.8392, −0.2678	5.7706, −0.8592	16.3673, −5.4000
90	−30.4270	−3.0250	−12.4001	−17.5244	−4.9643	1.8392, −0.2678	5.7706, −0.8592	16.3673, −5.4000

Table 3. The single particle energies for the bound and resonant states in ^{17}O varying with the grid number N_h of the Gauss-Hermite quadrature in Eq. (12). Here, the upper truncation $k_{\max} = 5.0$ fm^{-1} for the momentum integration and the grid number $N_l = 60$ for the Gauss-Legendre quadrature. All energies are in units of MeV.

N_h	$1s_{1/2}$ E	$2s_{1/2}$ E	$1p_{1/2}$ E	$1p_{3/2}$ E	$1d_{5/2}$ E	$1d_{3/2}$ E_r, E_i	$1f_{7/2}$ E_r, E_i	$1g_{9/2}$ E_r, E_i
20	−30.4270	−3.0249	−12.4001	−17.5244	−4.9643	1.8397, −0.2673	5.7697, −0.8574	16.3678, −5.4228
30	−30.4270	−3.0250	−12.4001	−17.5244	−4.9643	1.8392, −0.2678	5.7705, −0.8592	16.3675, −5.3982
40	−30.4270	−3.0250	−12.4001	−17.5244	−4.9643	1.8392, −0.2678	5.7706, −0.8592	16.3672, −5.4002
50	−30.4270	−3.0250	−12.4001	−17.5244	−4.9643	1.8392, −0.2678	5.7706, −0.8592	16.3674, −5.4000
60	−30.4270	−3.0250	−12.4001	−17.5244	−4.9643	1.8392, −0.2678	5.7706, −0.8592	16.3673, −5.4000
70	−30.4270	−3.0250	−12.4001	−17.5244	−4.9643	1.8392, −0.2678	5.7706, −0.8592	16.3673, −5.4000
80	−30.4270	−3.0250	−12.4001	−17.5244	−4.9643	1.8392, −0.2678	5.7706, −0.8592	16.3673, −5.4000
90	−30.4270	−3.0250	−12.4001	−17.5244	−4.9643	1.8392, −0.2678	5.7706, −0.8592	16.3673, −5.4000

Next, we check the dependence of the calculated results on the parameter N_l in the Gauss-Legendre quadrature with $k_{\max} = 5.0$ fm^{-1} and $N_h = 70$. The results are listed in Table 2. The convergence of the calculations on N_l is very good. For every bound or resonant state, the calculated energy tends to the same value with increasing N_l. When $N_l \geqslant 50$, the calculated results are unchanged with N_l at the present precision. This indicates that N_l = 60 is enough in the present calculations.

Finally, we check the dependence of the calculated results on the parameter N_h in the Gauss-Hermite quadrature with $k_{\max} = 5.0$ fm^{-1} and $N_l = 60$. The results are listed in Table 3. Similar to Table 2, the convergence of the calculations on N_l is excellent. With the increase of N_h from 20 to 90 by steps of 10, the calculated energy tends to the same value for every bound or resonant state. When $N_h \geqslant 60$, the calculated results no longer change with N_h at the present precision, which means that $N_h = 70$ is enough in the present calculations.

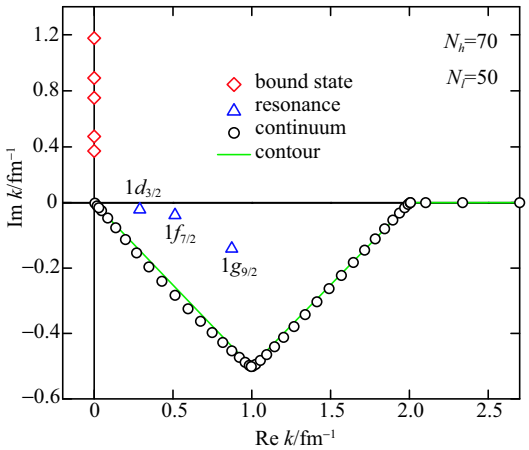

Fig. 3. (color online) The single-neutron spectra for ^{17}O in the complex momentum plane. The red open diamond, blue open triangle, and black open circles represent the bound states, the resonant states, and the continuum, respectively. The olive solid line is the contour of integration in the complex momentum plane.

Table 4. The calculated results for the bound states and resonant states in ^{17}O by using the complex momentum representation in comparison with those obtained in coordinate representation by the complex scaling method for resonances. E represents the energy of bound states. E_r and E_i represent respectively the real part and imaginary part ofthe energy for resonant states. All the units are MeV.

	momentum representation	coordinate representation
nl_j	$E(E_r, E_i)$	$E(E_r, E_i)$
$1s_{1/2}$	−30.4270	−30.4270
$1p_{1/2}$	−12.4001	−12.4001
$1p_{3/2}$	−17.5244	−17.5241
$1d_{5/2}$	−4.9643	−4.9645
$2s_{1/2}$	−3.0250	−3.0256
$1d_{3/2}$	1.8392, −0.2678	1.8099, −0.2215
$1f_{7/2}$	5.7706, −0.8592	5.8057, −0.8521
$1g_{9/2}$	16.3673, −5.4000	16.2711, −5.3530

Based on these considerations, we explore the bound and resonant states using the complex momentum representation method with the contour $k = 0$ fm^{-1}, k = 1.0–i0.5 fm^{-1}, $k = 2.0$ fm^{-1}, and $k_{\max} = 5.0$ fm^{-1}, and the grid numbers $N_l = 60$ and $N_h = 70$. The results are plotted in Fig. 3, where it can seen that all the bound states are on the imaginary axis in the complex momentum plane, while the resonant states are in the fourth quadrant. The continuum follows the contour. The bound and resonant states are separated clearly from the continuum.

The numerical results for the bound states and resonant states in Fig. 3 are listed in Table 4, comparing them with those obtained in the coordinate representation by the complex scaling method for resonances. From Table 4, the two calculations are in good agreement. The maximum relative deviation appears for the resonant state $1d_{3/2}$, which is less than 1.6% for the energy. The deviation does not affect our evaluation of

the resonance parameters. All these show that the results from the two methods are consistent in describing nuclear bound states and resonant states. Even so, the present result, as it is independent of any unphysical parameters, should be more accurate than those obtained by other methods.

4 Summary

Many methods have been developed for the calculation of nuclear resonances. Here, we have explored resonances by solving the Schrödinger equation in the complex momentum representation. We have presented in detail the theoretical formalism, and discussed the numerical details. With ^{17}O as an illustrative example, we have checked the dependence of the calculated results on the contour and found that all the bound and resonant states are independent of the contour as long as they are exposed in the complex momentum plane. We have demonstrated how to determine an appropriate contour for the momentum integration in order to obtain all the resonant states concerned. We have examined the dependence of the calculated results on the three unphysical parameters: the upper truncation of momentum integration $k_{\max}$, the grid number N_l in the Gauss-Legendre quadrature for momentum integration, and the grid number N_h in the Gauss-Hermite quadrature for coordinate integration. It is found that the convergence of the calculations on $k_{\max}$, N_l, and N_h is very good. When $k_{\max} \geqslant 4.0$ fm^{-1}, $N_l \geqslant 50$, and $N_h \geqslant 60$, the calculated results are unchanged at the present precision. We have calculated the bound states and resonant states in ^{17}O in comparison with those obtained by the complex scaling method in coordinate representation, and satisfactory agreement is obtained. The present results should be more accurate because they are independent of any unphysical parameters.

References

1 Wikipedia, https://en.wikipedia.org/wiki/Resonance
2 J. Meng and P. Ring, Rev. Lett., **77**: 3963 (1996)
3 W. Pöschl, D. Vretenar, G.A. Lalaziss, and P. Ring, Phys. Rev. Lett., **79**: 3841 (1997)
4 N. Sandulescu, N. Van Giai, and R.J. Liotta, Phys. Rev. C, **61**: 061301 (2000)
5 J. Meng and P. Ring, Phys. Rev. Lett., **80**: 460 (1998)
6 Y. Zhang, M. Matsuo, and J. Meng, Phys. Rev. C, **86**: 054318 (2012)
7 S. G. Zhou, J. Meng, P. Ring, and E. G. Zhao, Phys. Rev. C, **82**: 011301 (2010)
8 A. S. Jensen, K. Riisager, D. V. Fedorov, and E. Garrido, Rev. Mod. Phys., **76**: 215 (2004)
9 E. P. Wigner and L. Eisenbud, Phys. Rev., **72**: 29 (1947)
10 A. U. Hazi and H. S. Taylor, Phys. Rev. A, **1**: 1109 (1970)
11 J. R. Taylor, *Scattering Theory: The Quantum Theory on Nonrelativistic Collisions* (John Wiley & Sons, New York, 1972)
12 E. J. Heller and H. A. Yamani, Phys. Rev. A, **9**, 1201 (1974); E. J. Heller and H. A. Yamani, ibid. **9**: 1209 (1974)
13 V. I. Kukulin, V. M. Krasnopl'sky, and J. Horáček, *Theory of Resonances: Principles and Applications* (Kluwer, Dordrecht, 1989)
14 J. Humblet, B. W. Filippone, and S. E. Koonin, Phys. Rev. C, **44**: 2530 (1991)
15 B. N. Lu, E. G. Zhao, and S. G. Zhou, Phys. Rev. Lett., **109**: 072501 (2012)
16 B. N. Lu, E. G. Zhao, and S. G. Zhou, Phys. Rev. C, **88**: 024323 (2013)
17 E. N. Economou, *Green's Function in Quantum Physics* (Springer-Verlag, Berlin, 2006)
18 T. T. Sun, S. Q. Zhang, Y. Zhang, J. N. Hu, and J. Meng, Phys. Rev. C, **90**: 054321 (2014)
19 J. Aguilar and J. M. Combes, Commun. Math. Phys., **22**: 269 (1971); E. Balslev and J.M. Combes, Commun. Math. Phys., **22**: 280 (1971); B. Simon, Commun. Math. Phys, **27**: 1 (1972)
20 K. Arai, Phys. Rev. C, **74**: 064311 (2006)
21 N. Michel, W. Nazarewicz, M. Ploszajczak, and T. Vertse, J. Phys. G: Nucl. Part. Phys., **36**: 013101 (2009)
22 N. Michel, K. Matsuyanagi, and M. Stoitsov, Phys. Rev. C, **78**: 044319 (2008)
23 A. T. Kruppa, G. Papadimitriou, W. Nazarewicz, and N. Michel, Phys. Rev. C, **89**: 014330 (2014)
24 A. T. Kruppa, P. H. Heenen, H. Flocard, and R. J. Liotta, Phys. Rev. Lett., **79**: 2217 (1997)
25 N. Moiseyev, Phys. Rep., **302**: 212 (1998)
26 T. Myo, Y. Kikuchi, H. Masui, and K. Katō, Prog. Part. Nucl. Phys., **79**: 1 (2014)
27 J. Carbonell, A. Deltuva, A.C. Fonseca, and R. Lazauskas, Prog. Part. Nucl. Phys., **74**: 55 (2014)
28 J. Y. Guo, M. Yu, J. Wang, B. M. Yao, and P. Jiao, Comput. Phys. Commun., **181**: 550 (2010)
29 J. Y. Guo, X. Z. Fang, P. Jiao, J. Wang, and B. M. Yao, Phys. Rev. C, **82**: 034318 (2010)
30 Z. L. Zhu, Z. M. Niu, D. P. Li, Q. Liu, and J. Y. Guo, Phys. Rev. C, **89**: 034307 (2014)
31 M. Shi, Q. Liu, Z. M. Niu, and J. Y. Guo, Phys. Rev. C, **90**: 034319 (2014)
32 Q. Liu, J. Y. Guo, Z. M. Niu, and S. W. Wan, Phys. Rev. C, **86**: 054312 (2012)
33 L. Zhang, S. G. Zhou, J. Meng, and E. G. Zhou, Phys. Rev. C, **77**: 014312 (2008)
34 T. Berggren, Nucl. Phys. A, **109**: 265 (1968)
35 G. Hagen and J. S. Vaagen, Phys. Rev. C, **73**: 034321 (2006)
36 A. Deltuva, Few-Body Syst., **56**: 897 (2015)
37 C. V. Sukumar, J. Phys. A, **12**: 1715 (1979)
38 Y. R. Kwon and F. Tabakin, Phys. Rev., **18**: 932 (1978)
39 R. J. Liotta, E. Maglione, N. Sandulescu, T. Vertse, Phys. Lett. B, **367**: 1 (1996)
40 N. Michel, W. Nazarewicz, M. Ploszajczak, and K. Bennaceur Phys. Rev. Lett., **89**: 042502 (2002)
41 Niu Li, Min Shi, Jian-You Guo, Zhong-Ming Niu, and Haozhao Liang, Phys. Rev. Lett., **117**: 062502 (2016)
42 I. Hamamoto, Phys. Rev. C, **85**: 064329 (2012)
43 A. Bohr and B. R. Mottelson, Nuclear Structure (Benjamin, Reading, MA, 1969), Vol. I